Radio Science, Volume 13, Number 1, pages 131-138, January-February 1978

The forward scattering of microwave solar radiation from a water surface

F. J. Wentz

F. J. Wentz and Associates, Box 162, M.I.T. Branch P.O., Cambridge, Massachusetts 02139

(Received February 17, 1976.)

The forward scattering of microwave solar radiation from a smooth and from a rough water surface is computed. The smooth surface is assumed specular, and the rough surface is represented by a two-scale surface, for which two small-scale perturbation parameters, 0.10 and 0.25, are considered. The contribution of the scattered sunlight to the antenna temperature is found using the scalar approximation, and the results are compared with radiometer measurements of the Cape Cod Canal. The overall agreement is good, but in some cases the smooth-surface measurements are higher than the computations. This discrepancy possibly indicates an absolute calibration error or a slight misalignment of the antennas' boresights. The computations for the two perturbation parameters bracket the rough-surface measurements except when the sun's mirror image is far removed from the boresight direction. The small disagreement in this case may be due to a peaked large-scale slope distribution.

INTRODUCTION

If microwave radiometers are to sense accurately sea-surface temperature and roughness, then all important contributions to the antenna temperature must be taken into account. To determine the influence of sun glitter on the antenna temperature, *Swift* [1974] measured the forward scattering of sunlight from the Cape Cod Canal in Massachusetts. Data were collected at 1.4, 4.0, and 7.5 GHz for horizontal and vertical polarization while the antennas were fixed at a 40° nadir viewing angle. On May 17, 1972, the canal surface was relatively undisturbed, and the antenna temperatures rose significantly as the image of the sun passed through the antennas' main lobes and reached a maximum at 1516 EDT. On May 19 the canal surface was roughened by a 15 m/sec wind, and the rise in the antenna temperatures was considerably less than for the smooth surface.

In this paper we model Swift's sun-glitter experiment. The scalar approximation for the antenna temperature equation is used to compute the contribution of the forward-scattered sunlight to the antenna temperature. The smooth surface is assumed specular, and the rough surface is represented by a two-scale surface [*Wentz*, 1975*a*,*b*,*c*]. Two small-scale perturbation parameters, 0.10 and 0.25, are considered for the rough-surface computations. The antenna temperature measured in the absence of scattered sunlight is added to our computations in order to obtain the total antenna temperature. The results are plotted versus time and are compared with the measurements.

ANTENNA TEMPERATURE EQUATION

The mean canal surface defines the $z = 0$ plane of an x,y,z coordinate system, and the x axis corresponds to the azimuth direction of the antennas' boresights and is 245° east of true North. All vectors have unit magnitude, and the axis vectors are represented by $\mathbf{x}$, $\mathbf{y}$, and $\mathbf{z}$. An axial component of a vector is denoted by the superscript x, y, or z. The boresight vector $\mathbf{k}_b$, which points toward the surface, is then

$$\mathbf{k}_b = \mathbf{x} \sin 40° - \mathbf{z} \cos 40° \tag{1}$$

where 40° is the nadir viewing angle.

The following scalar approximation for the antenna temperature equation is used in the computations:

$$T_A(\mathbf{k}_b,P) = (4\pi)^{-1} \int\int dk_s^x\, dk_s^y\, G(\mathbf{k}_b,-\mathbf{k}_s) \cdot T_B(\mathbf{k}_s,\mathbf{P}_s)/|k_s^z| \tag{2}$$

$$\mathbf{P}_s = \begin{cases} \mathbf{k}_s \times \mathbf{z}/|\mathbf{k}_s \times \mathbf{z}|, & P = h \\ \mathbf{k}_s \times (\mathbf{k}_s \times \mathbf{z})/|\mathbf{k}_s \times \mathbf{z}|, & P = v \end{cases} \tag{3}$$

where $P = h$ or v represents observations for horizontal or vertical polarization, respectively. The

0048-6604/78/0102-0131$03.00

function $G(\mathbf{k}_b,-\mathbf{k}_s)$ is the antenna's gain in direction $-\mathbf{k}_s$, and $T_B(\mathbf{k}_s,\mathbf{P}_s)$ is the brightness temperature of the $\mathbf{P}_s$ polarization component of radiation propagating in direction $\mathbf{k}_s$. It should be noted that $dk_s^x\, dk_s^y/|k_s^z|$ is the differential solid angle. The gain function is assumed to have the scalar Kirchhoff form for an idealized parabolic reflector [*Jackson*, 1962], and the region of integration is confined to its main lobe.

$$G(\mathbf{k}_b,-\mathbf{k}_s) = [\csc\theta_b(1+\cos\theta_b)\,J_1(ka\sin\theta_b)]^2 \tag{4}$$

$$\cos\theta_b = -\mathbf{k}_s\cdot\mathbf{k}_b \tag{5}$$

where k is the radiation wavenumber and a is the radius of the reflector. The boresight gain is then

$$G(\mathbf{k}_b,\mathbf{k}_b) = (ka)^2 \tag{6}$$

The actual gain differs from the idealized gain for several reasons, which include nonuniform illumination by the feedhorn and spill-over. To account for these effects, we use the measured boresight gain to specify ka rather than use the radius of the reflector and the wavenumber. The boresight gains were measured to be 418, 548, and 497 for 1.4, 4.0, and 7.5 GHz, respectively (F. B. Beck, personal communication, 1975). The solar radiation entering the side lobes of the antennas contributed less than 0.5 K to the antenna temperatures because the side lobes that were directed toward the sun were at least 30 db less than the boresight gains.

BRIGHTNESS TEMPERATURE OF SCATTERED SUNLIGHT

The $\mathbf{P}_s$ polarization component of the brightness temperature of sunlight scattered in direction $\mathbf{k}_s$ from the canal surface is given by

$$T_B(\mathbf{k}_s,\mathbf{P}_s) = \int\int dk_i^x\, dk_i^y\, \Gamma(\mathbf{k}_i;\mathbf{k}_s,\mathbf{P}_s)\, T_\odot(\mathbf{k}_i) \tag{7}$$

where $T_\odot(\mathbf{k}_i)$ is the brightness temperature of the incident solar radiation having a propagation vector $\mathbf{k}_i$. The scattering function $\Gamma(\mathbf{k}_i;\mathbf{k}_s,\mathbf{P}_s)$ is defined in the next paragraph. We assume that the solar radiation is unpolarized and neglect the fact that in the 1.4 to 7.5 GHz region it is approximately 10% circularly polarized [*Aarons*, 1965]. We let $\psi_\odot$ denote the angular radius of the sun at microwave frequencies and let $\mathbf{k}_\odot$ denote the unit vector that points from the surface to the sun's center. The Rayleigh-Jeans approximation then gives

$$T_\odot(\mathbf{k}_i) = (F\lambda^2/2K)\,u(-\mathbf{k}_i\cdot\mathbf{k}_\odot - \cos\psi_\odot) \div [2\pi(1-\cos\psi_\odot)] \tag{8}$$

where F is the incident solar flux, λ is the radiation wavelength, and K is Boltzmann's constant. The unit step function u limits the integration region for (7) to the solid angle subtended by the sun, and the bracketed term equals this solid angle. The angular radius $\psi_\odot$ at 1.4 to 7.5 GHz is taken to be 0.293°, which is 10% greater than the optical angular radius [*Aarons*, 1965]. The Sagamore Hill Radio Observatory located in Hamilton, Massachusetts, made solar flux measurements at 1.415, 2.695, 4.995, and 8.800 GHz on May 17 and 19, 1972 (J. Aarons, personal communication, 1975). Linear interpolations of these flux measurements provide the 1.4, 4.0, and 7.5 GHz values for F. These interpolated values appear in Table 1 along with the corresponding brightness temperatures $T_\odot$. The sun vector $\mathbf{k}_\odot$ is found as a function of time from *Swift's* [1974] plot of the sun's elevation and azimuth angles.

The scattering function $\Gamma(\mathbf{k}_i;\mathbf{k}_s,\mathbf{P}_s)$ is the sum of the scattering coefficients for two orthogonal incident polarizations.

$$\Gamma(\mathbf{k}_i;\mathbf{k}_s,\mathbf{P}_s) = \Gamma(\mathbf{k}_i,\mathbf{P}_{i1};\mathbf{k}_s,\mathbf{P}_s) + \Gamma(\mathbf{k}_i,\mathbf{P}_{i2};\mathbf{k}_s,\mathbf{P}_s) \tag{9}$$

$$\mathbf{P}_{i1}\cdot\mathbf{P}_{i2}^* = 0 \tag{10}$$

where the superscript * denotes complex conjugate. The definition of scattering coefficient used herein is the ratio of the power density function $\Omega(\mathbf{k}_s,\mathbf{P}_s)$ to the time-averaged $\mathbf{P}_i$ polarization component of the incident power having a propagation vector $\mathbf{k}_i$. The quantity $\Omega(\mathbf{k}_s,\mathbf{P}_s)\, dk_s^x\, dk_s^y$ is the time-averaged $\mathbf{P}_s$ polarization component of scattered power having a propagation vector in the neighborhood $dk_s^x\, dk_s^y$ of $\mathbf{k}_s$. The scattering coefficient defined by *Peake* [1959] is in terms of power scattered per solid angle and is found by multiplying our coefficient by $4\pi k_s^z$.

The scattering coefficients are computed using

TABLE 1. Incident solar flux and brightness temperature.

Frequency (GHz)	May 17—Smooth F (10^{-22} joules/m^2)	May 17—Smooth $T_\odot$ (K)	May 19—Rough F (10^{-22} joules/m^2)	May 19—Rough $T_\odot$ (K)
1.4	99	192,000	96	186,000
4.0	184	46,000	169	42,000
7.5	267	19,000	254	18,000

a two-scale scattering model [*Wentz*, 1975*b*]. Besides the explicit arguments, the scattering coefficients are functions of the following: (1) the frequency f of the observed radiation, (2) the surface permittivity ϵ, (3) the probability density function (pdf) $p(n^x,n^y)$ for the large-scale surface normal **n**, and (4) the small-scale isotropic power spectrum $W(\kappa)$, where κ is the sea wavenumber. The permittivity ϵ depends on the water temperature and salinity and on f. The water temperatures for the smooth and rough surfaces were measured to be 287.8 and 288.2 K, respectively. Conductivity measurements yielded a constant 28‰ for the water salinity. Expressions derived by *Klein and Swift* [1977] are used to calculate ϵ for the three frequencies and two water temperatures, and the results appear in Table 2.

The canal surface on May 17 was described as near-specular, and the wavestaff record was virtually level. In view of this, a specular surface is assumed and the roughness distributions are simply

$$p(n^x,n^y) = \delta(n^x)\,\delta(n^y) \tag{11}$$

$$W(\kappa) = 0 \tag{12}$$

where δ is the Dirac delta function. For the rough-surface case, the power spectrum $S(\kappa)$ reported by *Wentz* [1975*a*] is used to specify $p(n^x,n^y)$ and $W(\kappa)$. This power spectrum is based in part on ground-truth data collected on May 25 when a 14 m/sec easterly wind prevailed, and it is probably representative of the surface roughness on May 19 when a 15 m/sec easterly wind prevailed. The capillary portion of the spectrum is found by calculating the friction velocity U from expressions given by *Cardone* [1969]. The wind speed was measured at 58 m above the surface and, by assuming a neutral atmosphere, one obtains $U = 51$ cm/sec for a 14 m/sec wind. This result in then inserted in *Pierson and Stacy's* [1973] expressions for the isotropic power spectrum of capillary waves. In terms of cm^3, these expressions are given by

$$S(\kappa) = 0.00405\,D\kappa_3^{-d}\kappa^{d-3}, \quad \kappa_2 \le \kappa < \kappa_3 \tag{13}$$

TABLE 2. Permittivity of canal water.

Frequency	Permittivity ϵ 287.8 K—Smooth	288.2 K—Rough
1.4 GHz	$74.96 - 51.71j$	$74.86 - 52.03j$
4.0 GHz	$70.11 - 33.65j$	$70.12 - 33.58j$
7.5 GHz	$60.34 - 36.21j$	$60.52 - 36.05j$

$$S(\kappa) = 0.00405\,D\kappa^{-3}, \quad \kappa_3 \le \kappa < \kappa_4 \tag{14}$$

$$S(\kappa) = 0.00405\,D\kappa_4^6\kappa^{-9}, \quad \kappa_4 \le \kappa \tag{15}$$

$$D = (1.247 + 0.0268\,U + 6.03 \times 10^{-5}\,U^2)^2 \tag{16}$$

$$d = \log(12\,D/U)/\log(\kappa_3/\kappa_2) \tag{17}$$

$$\kappa_4 = 2.09(U^3/D)^{1/6} \tag{18}$$

where $\kappa_2 = 0.359$ cm^{-1} and $\kappa_3 = 0.942$ cm^{-1}. One should note that Cardone's expressions are for an open sea and the Pierson-Stacy expressions are based on wind-water tunnel measurements. Applying these expressions to a canal possibly introduces significant error. Also, the assumption of an isotropic spectrum is unrealistic but is made because information about the directional properties of a wind-driven water surface is limited, especially for a canal with an appreciable current. The gravity power spectrum for which $\kappa \le 10^{-3}$ cm^{-1} was measured by a laser profilometer and by a wavestaff. This ground-truth spectrum is connected to the capillary spectrum by drawing a straight line on a log $S(\kappa)$ versus log κ plot. This interpolation is given by

$$S(\kappa) = S(\kappa_1)(\kappa_1/\kappa)^t, \quad \kappa_1 \le \kappa < \kappa_2 \tag{19}$$

$$t = \log[S(\kappa_1)/S(\kappa_2)]/\log(\kappa_2/\kappa_1) \tag{20}$$

where $\kappa_1 = 10^{-3}$ cm^{-1} and $S(\kappa_2)$ is given by (13). The laser profilometer measured $S(\kappa_1)$ to be 1.2×10^3 cm^3. The spectrum for $\kappa < \kappa_1$ can be empirically found from the laser data, but this is not necessary because inspection shows that this portion of the spectrum contributes less than 10^{-5} to the slope variance and has no effect on the computations.

The spectrum $S(\kappa)$ is divided into a large-scale spectrum $S_l(\kappa)$ and a small-scale spectrum $S_s(\kappa)$.

$$S_l(\kappa) = \begin{cases} S(\kappa), & \kappa \le \kappa_c \\ 0, & \kappa > \kappa_c \end{cases} \tag{21}$$

$$S_s(\kappa) = \begin{cases} 0, & \kappa \le \kappa_c \\ S(\kappa), & \kappa > \kappa_c \end{cases} \tag{22}$$

where $W(\kappa)$ is related to $S_s(\kappa)$ by

$$W(\kappa) = (2/\pi)\,S_s(\kappa)/\kappa \tag{23}$$

The value of the cutoff wavenumber κ_c is found by assigning a value to the small-scale perturbation parameter $k\zeta$, where ζ is the rms height variation on the small-scale surface. Integrating over the

small-scale spectrum gives ζ.

$$\zeta^2 = \int_{\kappa_c}^{\infty} d\kappa\, S(\kappa) \tag{24}$$

The above integral is evaluated in closed form, ζ being expressed as a function of κ_c. The inverse of this function then gives κ_c in terms of ζ. Perturbation theory requires that $k\zeta$ be small in comparison to unity, and setting $k\zeta$ equal to zero results in the two-scale model degenerating to geometric optics. To study the effect of variations of $k\zeta$ on the computations, we consider two intermediate values, 0.10 and 0.25. Once κ_c is determined, the large-scale slope variance $\langle Z^2 \rangle$ is calculated from

$$\langle Z^2 \rangle = \int_0^{\kappa_c} d\kappa\, \kappa^2\, S(\kappa) \tag{25}$$

Table 3 contains the values of κ_c and $\langle Z^2 \rangle$ for the three frequencies and two perturbation parameters.

The large-scale slope pdf is approximated by a gaussian distribution [*Cox and Munk*, 1956].

$$p_z(Z_x, Z_y) = (\pi \langle Z^2 \rangle)^{-1} \exp[-(Z_x^2 + Z_y^2)/\langle Z^2 \rangle] \tag{26}$$

$$Z_x = -n^x/n^z \tag{27}$$

$$Z_y = -n^y/n^z \tag{28}$$

The relationship between the surface normal pdf and the surface slope pdf is

$$p(n^x, n^y) = p_z(Z_x, Z_y)/(n^z)^4 \tag{29}$$

where $(n^z)^4$ is the Jacobian relating the Z_x, Z_y coordinates to the n^x, n^y coordinates.

The scattering coefficient is a sum of two terms, one associated with the incoherent scattered power (subscript $\times$) and the other with the coherent reflected power (subscript $\bigcirc$).

$$\Gamma(\mathbf{k}_i, \mathbf{P}_i; \mathbf{k}_s, \mathbf{P}_s) = \Gamma_\times(\mathbf{k}_i, \mathbf{P}_i; \mathbf{k}_s, \mathbf{P}_s) + \Gamma_\bigcirc(\mathbf{k}_i, \mathbf{P}_i; \mathbf{k}_s, \mathbf{P}_s) \tag{30}$$

TABLE 3. Cutoff sea wavenumber and large-scale slope variance.

Frequency	κ_c (cm^{-1})		$\langle Z^2 \rangle$	
	$k\zeta = 0.10$	$k\zeta = 0.25$	$k\zeta = 0.10$	$k\zeta = 0.25$
1.4 GHz	3.0×10^{-1}	2.5×10^{-2}	8.1×10^{-3}	1.4×10^{-4}
4.0 GHz	1.0×10^{0}	3.6×10^{-1}	3.6×10^{-2}	1.1×10^{-2}
7.5 GHz	1.9×10^{0}	7.7×10^{-1}	5.6×10^{-2}	2.7×10^{-2}

The incoherent term is given by an integral over the surface normal pdf, and $W(\kappa)$ appears in the integrand. The sea wavenumber argument for this integration is

$$\kappa = k|(\mathbf{k}_s - \mathbf{k}_i) - [(\mathbf{k}_s - \mathbf{k}_i) \cdot \mathbf{n}]\mathbf{n}| \tag{31}$$

The argument goes to zero as $\mathbf{k}_s$ approaches the reflection propagation vector $\mathbf{k}_r$.

$$\mathbf{k}_r = \mathbf{k}_i - 2(\mathbf{k}_i \cdot \mathbf{n})\mathbf{n} \tag{32}$$

Since $W(\kappa)$ is zero for $\kappa \leq \kappa_c$, the integrand is zero when the scatter direction is in the vicinity of the reflection direction. For this reason the incoherent term is small compared to the coherent term in the case of forward scattering. Approximate computations show that the contribution of the incoherent scattered sunlight to the brightness temperature is negligible for 4.0 and 7.5 GHz, being less than 0.1 K. At 1.4 GHz the incoherent contribution is about 4 K, but this is much smaller than the observed rise in the antenna temperature. This rise ranged from 30 to 165 K for the observation period being considered. Thus, according to the two-scale model, incoherent scattering is of minor significance, and we simplify the problem by setting $\Gamma_\times(\mathbf{k}_i, \mathbf{P}_i; \mathbf{k}_s, \mathbf{P}_s)$ to zero.

The surface roughness was not too severe, and shadowing of the incident radiation and multiple reflections by the forward-scattered radiation are negligible for the incidence and scatter angles being considered. The coherent scattering coefficient for single reflections from an unshadowed surface is given by *Wentz* [1975*b*] to be

$$\Gamma_\bigcirc(\mathbf{k}_i, \mathbf{P}_i; \mathbf{k}_s, \mathbf{P}_s) = p(n^x_\bigcirc, n^y_\bigcirc)|\mathbf{P}_i \cdot [(\mathbf{P}_s^* \cdot \mathbf{H}_s)R_h\mathbf{H}_i + (\mathbf{P}_s^* \cdot \mathbf{V}_s)R_v\mathbf{V}_i]|^2/|4k_s^z k_i^z| \tag{33}$$

$$\mathbf{n}_\bigcirc = (\mathbf{k}_s - \mathbf{k}_i)/|\mathbf{k}_s - \mathbf{k}_i| \tag{34}$$

$$\mathbf{H}_m = \mathbf{k}_m \times \mathbf{n}_\bigcirc/|\mathbf{k}_m \times \mathbf{n}_\bigcirc| \tag{35}$$

$$\mathbf{V}_m = \mathbf{k}_m \times \mathbf{H}_m \tag{36}$$

where $m = i$ or s. The horizontal and vertical reflection coefficients, R_h and R_v, are modifications of the Fresnel reflection coefficients and account for the reduction in reflected power due to incoherent scattering. They are functions of $\mathbf{k}_i \cdot \mathbf{n}_\bigcirc$, ϵ, k, and $W(\kappa)$ [*Wentz*, 1975*b*]. When the perturbation parameter is 0.10, the reduction in reflected power is practically negligible, being about 3%, and when the perturbation parameter is 0.25, the reduc-

tion is about 15%. The sum of the scattering coefficients for two orthogonal incident polarizations appears in (7) and is given by

$$\Gamma(\mathbf{k}_i;\mathbf{k}_s,\mathbf{P}_s) = p(n_{\bigcirc}^x, n_{\bigcirc}^y)(|\mathbf{P}_s^* \cdot \mathbf{H}_s|^2 |R_h|^2 + |\mathbf{P}_s^* \cdot \mathbf{V}_s|^2 |R_v|^2)/|4k_s^z k_i^z| \quad (37)$$

ANTENNA TEMPERATURE IN THE ABSENCE OF SCATTERED SUNLIGHT

In order to compute the total antenna temperature T_A, we add the antenna temperature in the absence of scattered sunlight to $T_A(\mathbf{k}_b,P)$ given by (2). To do this for the rough surface, we use radiometer observations taken between 1840 and 1852 EDT on May 25. Both computations and measurements show that at this time the scattered sunlight is no longer a significant factor. The major contributor to T_A for these measurements is emission from the rough water surface. As mentioned in the last section, the wind that prevailed during these late afternoon emission observations was nearly the same as that for the scattered sunlight observations, and probably the rough-surface emissivities for the two sets of measurements are about equal. The water temperature for the emission observations was 2.1 K colder than that for the scattered sunlight observations. A small correction is made to compensate for this difference, and the quantity that is added to $T_A(\mathbf{k}_b,P)$ is

$$\bar{T}_A = T_A^e + 2.1(T_A^e / T_w^e) \quad (38)$$

where T_A^e and T_w^e are the antenna temperature at a 40° nadir angle and the water temperature for the emission observations. The term in the parentheses is a fair approximation for the rough-surface emissivity. Another contributor to T_A is the cosmic and atmospheric radiation that is scattered from the canal surface. For clear skies and a 40° nadir angle, this scattered radiation adds about 4 K to T_A in the 1.4 to 7.5 GHz region [*Wentz*, 1975*a*]. Clear skies were present for the emission observations, but a fog had developed just prior to the scattered sunlight observations. We neglect this difference in atmospheric conditions, and possibly the computations have a small negative bias.

For the smooth-surface case the antenna temperature $\bar{T}_A$ in the absence of scattered sunlight is found from radiometer measurements made between 0126 and 0138 on May 26. During these observations the surface was slick, and the water temperature was 3.9 K colder than that for the sun reflection observations. Equation (38) is again used to find $\bar{T}_A$ except that 3.9 replaces 2.1. No measurements were reported for horizontal polarization at 1.4 GHz, and in this particular case the brightness temperature $(T_B)_{sp}$ of a specular water surface is used to specify $\bar{T}_A$.

TABLE 4. Antenna temperature in the absence of scattered sunlight.

	$\bar{T}_A$			
	Horizontal polarization		Vertical polarization	
Frequency	Smooth	Rough	Smooth	Rough
1.4 GHz	84.1 K	87.6 K	120.9 K	-
4.0 GHz	89.7 K	95.2 K	126.7 K	131.0 K
7.5 GHz	89.2 K	96.2 K	131.8 K	136.0 K

$$(T_B)_{sp} = \xi_{sp} T_w + (1 - \xi_{sp}) T_d \quad (39)$$

where T_w is the water temperature appearing in Table 2 and ξ_{sp} is the specular emissivity that is calculated from the permittivity also appearing in Table 2. The downward brightness temperature T_d is taken to be 6 K [*Wentz*, 1975*a*], which corresponds to the clear sky condition that was present during both sets of smooth-surface observations. The smooth- and rough-surface values for $\bar{T}_A$ appear in Table 4. The 1.4 GHz, vertically polarized measurements of the sunlight scattering from the rough surface were not reported, and the corresponding computations are not done.

RESULTS

The total antenna temperature T_A is plotted versus time in Figures 1 and 2 for horizontal and vertical polarization, respectively. The circles and triangles represent the smooth- and rough-surface measurements, respectively. The solid curves show the specular-surface computations, and the large-dashed and small-dashed curves show the rough-surface computations for a 0.10 and a 0.25 perturbation parameter, respectively. Both the measurements and computations reach a maximum near 1516 EDT. At this time the antennas' boresights point most closely toward the sun's mirror image. The solar brightness temperature increases dramatically with decreasing frequency in the 1.4 to 7.5 GHz region. The rise in antenna temperature shows the same frequency dependence, and the 1.4 GHz, horizontally polarized radiation from the smooth

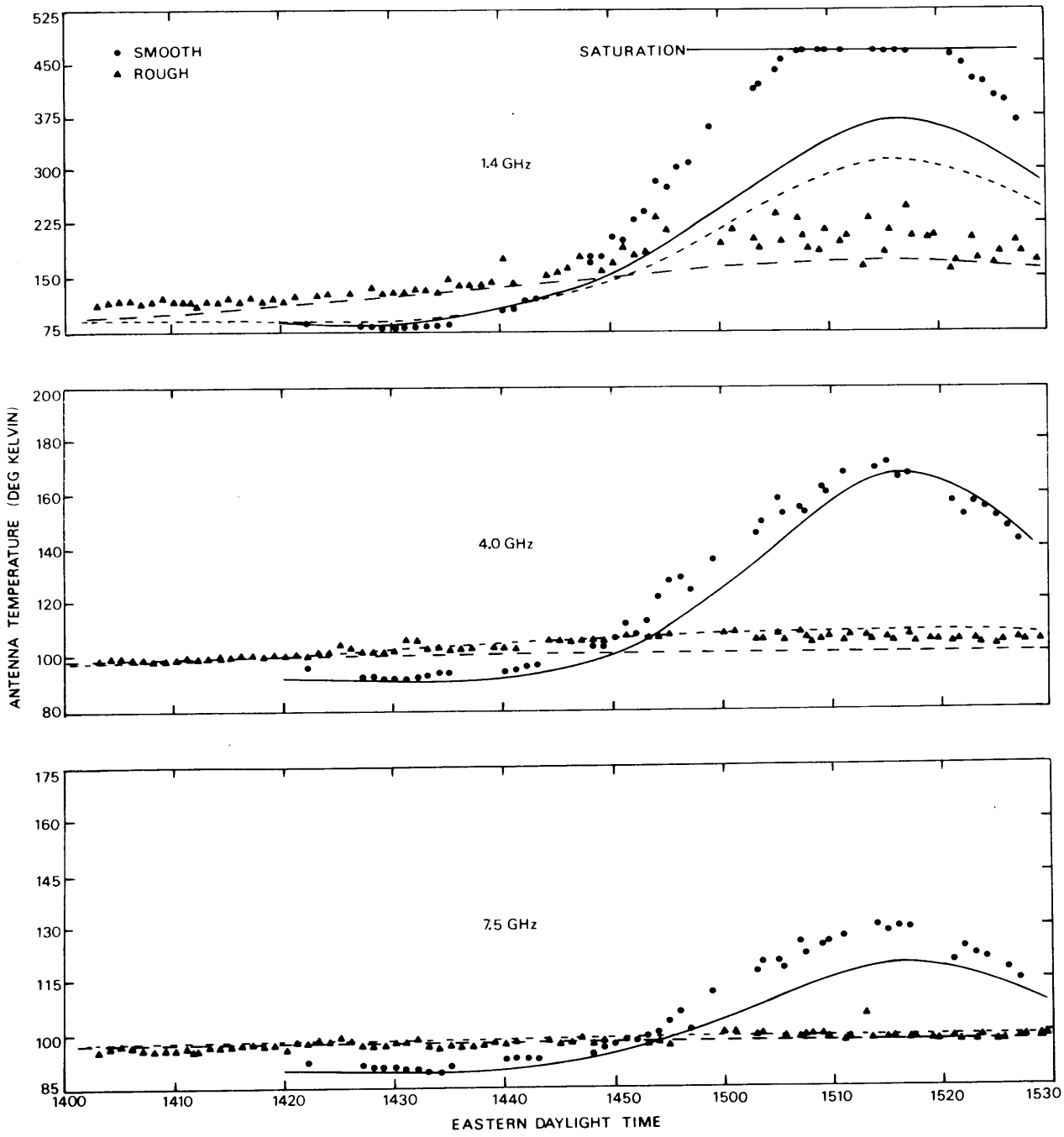

Fig. 1. The antenna temperature versus time for horizontal polarization.

surface saturates the radiometer.

The 1.4 GHz measurements of the smooth surface rise considerably above the computations. Part of this disagreement may be due to an error in specifying the boresight direction. The good agreement on the time of maximum response indicates that the boresight error probably does not exceed 1°, but a 1° error translates into about a 50 K error in the maximum T_A. Also, the radiometer was operating well outside its absolute calibration range,

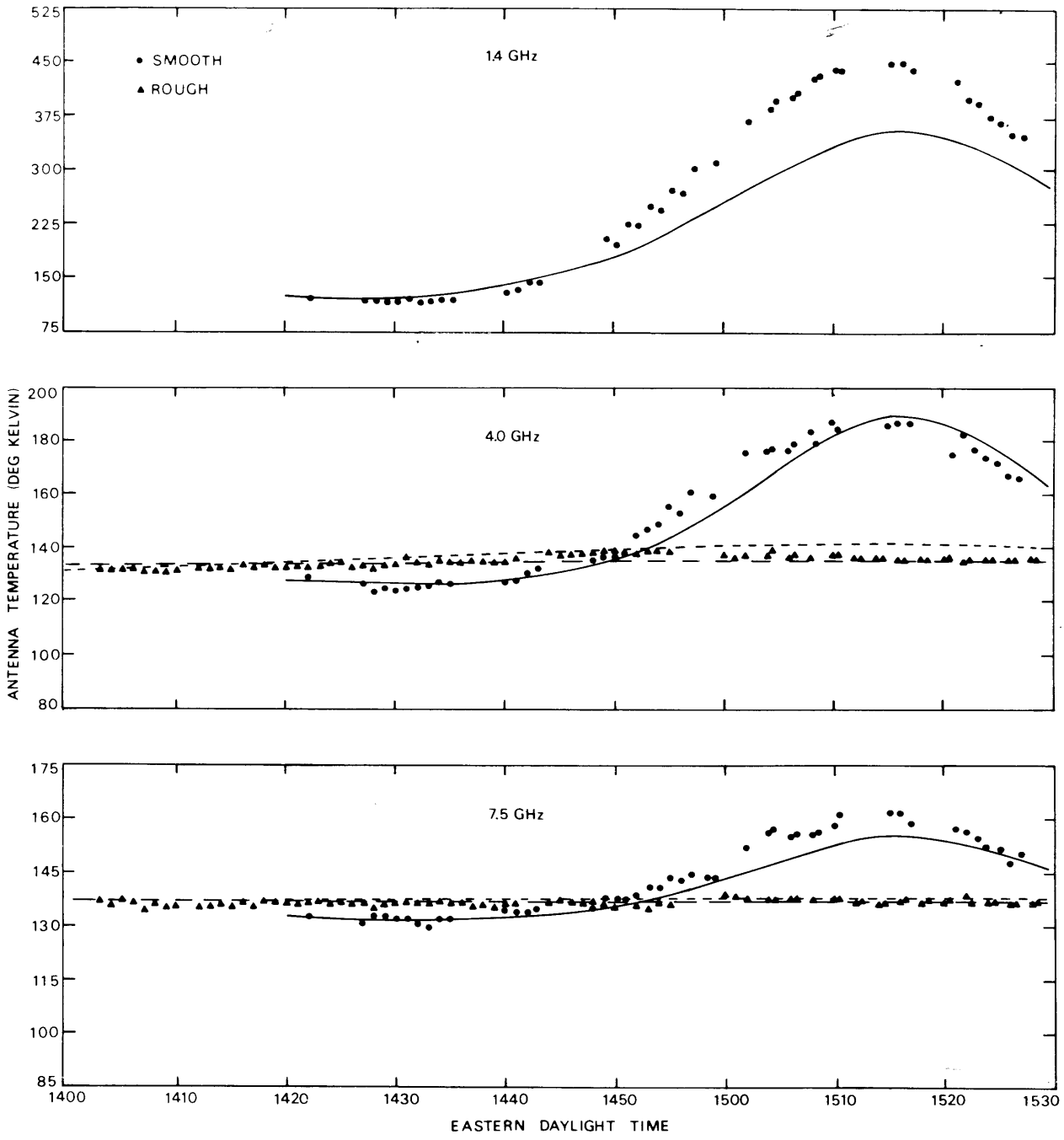

Fig. 2. The antenna temperature versus time for vertical polarization.

and a large experimental error could have resulted. At 4.0 GHz the agreement for the smooth surface is good, and at 7.5 GHz the measurements again exceed the computations. The specification of the 7.5 GHz solar flux is based on a linear interpolation between 5 and 8.8 GHz. This relatively large interpolation may cause some error.

For the rough-surface case the large-scale slope variance depends on the choice of the perturbation parameter $k\zeta$ because more of the sea spectrum

is considered large scale when the smaller $k\zeta$ is chosen. This dependence is the principal cause of the difference between the $k\zeta = 0.10$ and 0.25 curves. These two curves nicely bracket the rough-surface measurements except at 1.4 GHz between 1400 and 1500 EDT. In this case the computations seem too low. One possible explanation for this disagreement is that the probability of very steep slopes is greater than gaussian. That is to say, the large-scale slope pdf is peaked, and both *Cox and Munk's* [1956] sun-glitter observations and *Wu's* [1971] wind-water tunnel measurements support this assertion. This nongaussian effect would not be noticeable at the two higher frequencies because the solar brightness temperature is too small.

Acknowledgments. This research was supported by NASA Langley under contract L-34351A. I wish to thank W. L. Jones and J. W. Johnson for their assistance and am especially grateful to C. T. Swift and F. B. Beck for supplying necessary data, all of whom are with the NASA Langley Research Center. I also wish to thank J. Aarons of Air Force Cambridge Research Laboratories for providing the solar flux measurements.

REFERENCES

Aarons, J. (1965), *Solar System Radio Astronomy*, pp. 49-85, Plenum, New York.

Cardone, V. J. (1969), Specification of the wind field distribution in the marine boundary layer for wave forecasting, *Rep. TR 69-1*, Geophysical Sciences Laboratory, New York University, New York.

Cox, C., and W. Munk (1956), Slopes of the sea surface deduced from photographs of sun glitter, *Bull. Scripps Inst. Oceanogr.*, *6*, 401-488.

Jackson, J. D. (1962), *Classical Electrodynamics*, p. 296, John Wiley, New York.

Klein, L. A., and C. T. Swift (1977), An improved model for the dielectric constant of sea water at microwave frequencies, *IEEE Trans. Antennas Propagat.*, *AP-25*, 104-111.

Peake, W. H. (1959), Interaction of electromagnetic waves with some natural surfaces, *IRE Trans. Antennas Propagat*, *AP-7*(spec. suppl.), S324-S329.

Pierson, W. J., and R. A. Stacy (1973), The elevation, slope, and curvature spectra of a wind-roughened sea surface, *Contract. Rep. NASA CR-2247*, p. 15, NASA Langley Research Center, Hampton, Virginia 23665.

Swift, C. T. (1974), Microwave radiometer measurements of the Cape Cod Canal, *Radio Sci.*, *9*, 641-653.

Wentz, F. J. (1975*a*), Computation of theoretical brightness temperatures corresponding to the Cape Cod Canal radiometer measurements, *Contract. Rep. L-24420A, Part I*, 12 pp., NASA Langley Research Center, Hampton, Virginia 23665.

Wentz, F. J. (1975*b*), Radar backscattering from a sea having an anisotropic large-scale surface, *Contract. Rep. L-24420A, Part II*, 34 pp., NASA Langley Research Center, Hampton, Virginia 23665.

Wentz, F. J. (1975*c*), A two-scale scattering model for foam-free sea microwave brightness temperatures, *J. Geophys. Res.*, *80*, 3441-3446.

Wu, J. (1971), Slope and curvature distributions of wind-disturbed water surface, *J. Opt. Soc. Amer.*, *61*, 852-858.